catalysts

MDPI

Article

Role of Post-Hydrothermal Treatment on the Microstructures and Photocatalytic Activity of TiO_2-Based Nanotubes

Mohammad Qamar [1,*], Shabi Abbas Zaidi [2], Mohd Rafatullah [3,*], Mohammad Qutob [3], Sun-Jae Kim [4] and Qasem A. Drmosh [1]

[1] Interdisciplinary Research Center for Hydrogen and Energy Storage, King Fahd University of Petroleum and Minerals, Dhahran 31261, Saudi Arabia; drmosh@kfupm.edu.sa
[2] Analytical Chemistry Program, Department of Chemistry and Earth Sciences, College of Arts and Sciences, Qatar University, Doha P.O. Box 2713, Qatar; shabizaidi@qu.edu.qa
[3] School of Industrial Technology, Universiti Sains Malaysia (USM), George Town 11800, Penang, Malaysia; mohammadisamqutob@student.usm.my
[4] Department of Nanotechnology and Advanced Materials Engineering, Sejong University, Seoul 05006, Korea; sjkim1@sejong.ac.kr
* Correspondence: qamar@kfupm.edu.sa (M.Q.); mrafatullah@usm.my (M.R.)

Abstract: The present study demonstrates the thermal stability and photocatalytic activity of TiO_2-based nanotubes with respect to post-hydrothermal treatment. Titanate nanotubes were synthesized by adapting an alkali hydrothermal method from TiO_2 sol using NaOH as a catalyst. The effect of post-hydrothermal heating on the properties—such as structure, morphology, textural properties, and activity—of as-synthesized one-dimensional titania nanostructure is investigated in detail. The characterizations are carried out using SEM, EDX, TEM, XRD, and a BET surface area analyzer. When heated in the presence of water in an autoclave, the protonated titanate phase of the nanotubes converts to anatase phase. Meanwhile, the tubular morphology is gradually lost as the post-hydrothermal heating duration increases. The photocatalytic activity was assessed utilizing the photo-oxidation of an amaranth dye. It is discerned that the as-prepared nanotubes are photocatalytically inactive but become active after post-hydrothermal processing. The activity trend follows the formation of the active phase—the titanate phase crystallizes into a photocatalytically-active anatase phase during post-hydrothermal heating. The effect of experimental parameters, such as reaction pH, dye concentration, and amount of catalyst, on the dye removal is studied. The findings also highlight that the role of holes/$OH^{\bullet}$ is more prominent as compared to conduction band electron/$O_2^{-\bullet}$ for the removal of the dye. In addition, the photocatalyst exhibited excellent stability and reusability.

Keywords: titanium dioxide; titanate; nanotubes; hydrothermal synthesis; photocatalysis

Citation: Qamar, M.; Zaidi, S.A.; Rafatullah, M.; Qutob, M.; Kim, S.-J.; Drmosh, Q.A. Role of Post-Hydrothermal Treatment on the Microstructures and Photocatalytic Activity of TiO_2-Based Nanotubes. *Catalysts* **2022**, *12*, 702. https://doi.org/10.3390/catal12070702

Academic Editor: Simonetta Palmas

Received: 3 June 2022
Accepted: 24 June 2022
Published: 27 June 2022

1. Introduction

Nanotubes have been a popular one-dimensional allotropic form of carbon in the scientific domain. Currently, a wide variety of nanotubes composed of various different elements, such as carbon, titanium, tungsten, zinc, etc., have attracted the attention of scientists [1–4]. It has been established that a wide range of layered materials can form nanotubes since the discovery of nanotube morphology [5]. Of such materials, titanate nanotubes or TiO_2-based nanotubes have shown tremendous potential in diverse applications [6,7] such as environmental threats including water pollution, impacts on marine ecosystems, and livestock wastes that are on the forefront among various other global issues [8,9].

Substantial work has been performed over the last several decades to develop novel materials with an aim to improve photocatalytic activity or to find additional ways to improve the effectiveness of existing photocatalysts [10,11]. It has now been established that by controlling photocatalyst features, such as morphology, shape, size, surface area and its functionalization, and so forth, the photocatalytic activity can be significantly improved [12–16].

Therefore, because of their increased surface area and one-dimensional shape, TiO_2 are expected to be a feasible strategy, which offers an effective delocalization method for the charge carriers. Owing to many peculiar characteristics, such high charge-discharge capacity, excellent photocatalytic ability and high surface area, these one-dimensional nanostructures have been employed in electrochemical energy storage systems [17,18] in addition to in photovoltaics and semiconductor photocatalysts as well as catalysts support and gas sensors [19–21]. To produce one-dimensional nanostructures of TiO_2 (initially called needle-like structures), Kasuga et al. revealed an alkali hydrothermal process [22]. The method is simple, low cost and capable of producing the product in large quantities.

Since the structure of nanotubes produced by the alkali hydrothermal process is similar to that of titanium oxide, the photocatalysis can be one of the most potential applications of TiO_2-based nanotubes. However, not much information about the effect of post-hydrothermal treatment on the phase change and photocatalytic performance is available. For instance, TiO_2 nanotubes and Fe-, Ni-, Co- and Pt co-doped TiO_2 nanotubes were prepared and the photodecomposition of a mixture of NH_3, CH_4, and CO_2 was investigated [23]. In another study, Kim et al. prepared a heterostructure consisting of TiO_2 nanotubes and ultrathin 2D $ZnIn_2S_4$ nanosheets, and demonstrated efficient and selective photocatalytic CO_2 reduction [24]. The surface of TiO_2 nanotubes was also modified with g-C_3N_4 for enhanced photocatalytic reduction of CO_2 to CH_4 and CO [25]. Peng et al. fabricated PbS nanocrystal-sensitized ultrafine TiO_2 nanotubes for efficient and unusual broadband-light-driven hydrogen production [26]. More examples can be presented here to highlight the fact that as-prepared TiO_2 nanotubes have been used as-is or in the form of nanocomposites for photocatalytic applications [27–30]. However, it should be noted that the as-prepared TiO_2 nanotubes are photocatalytically-inactive because of their titanate structures. Earlier, our group discussed and confirmed the phase and structural composition of the needle-like morphology, which was produced through a sodium hydroxide-mediated alkali process [31].

The findings of this study suggest that the photocatalytic activity in TiO_2-based nanotubes can be generated with post-hydrothermal heat treatment, and this can be highly advantageous in designing nanocomposites with TiO_2-based nanotubes. The present study demonstrates the impact of post-hydrothermal heating time on: (1) the structural and the morphological transformations; and (2) the photocatalytic activity of the TiO_2-based nanotubes. The post-hydrothermal temperature was kept constant (120 °C), while the heating time was varied between 1 and 24 h. Structural and morphological evolution was followed by XRD and microscopic techniques. The photocatalytic activity has been investigated by studying the degradation rate of amaranth dye as a probe reaction. Furthermore, the degradation rate of the dye has been obtained by varying reaction pH (between ~3.5 and ~10.5), substrate (dye) concentration (between 0.15 and 0.70 mM), and catalyst loadings (between 0.5 and 5 g L^{-1}). In addition, the role of holes/$OH^{\bullet}$ and conduction band electron/$O_2^{-\bullet}$ for the removal of the dye were investigated. In addition, the photocatalyst exhibited excellent stability and reusability. Photocatalytic experiments were carried out to investigate the stability and the recyclability of the photocatalytic sample.

2. Results and Discussion

Figure 1a depicts that, after acid treatment, the as-prepared nanotubes possess tri-titanate phase structure with monoclinic symmetry, as previously reported [32]. The ion-exchange process shows a significant influence on the molecular structure of the samples. The XRD patterns of the acid-treated samples differ slightly than those of the untreated. The intensity of the reflections near 10° and 28°, which correspond to (200) and (211) reflections, are substantially reduced after ion-exchange. This is presumably due to different scattering characteristics of the ions (Na^+/H^+) [31]. Energy dispersive X-ray (EDX) analyses (Figure 1b) indicated that the sodium ions were significantly removed from the as-prepared nanotubes samples.

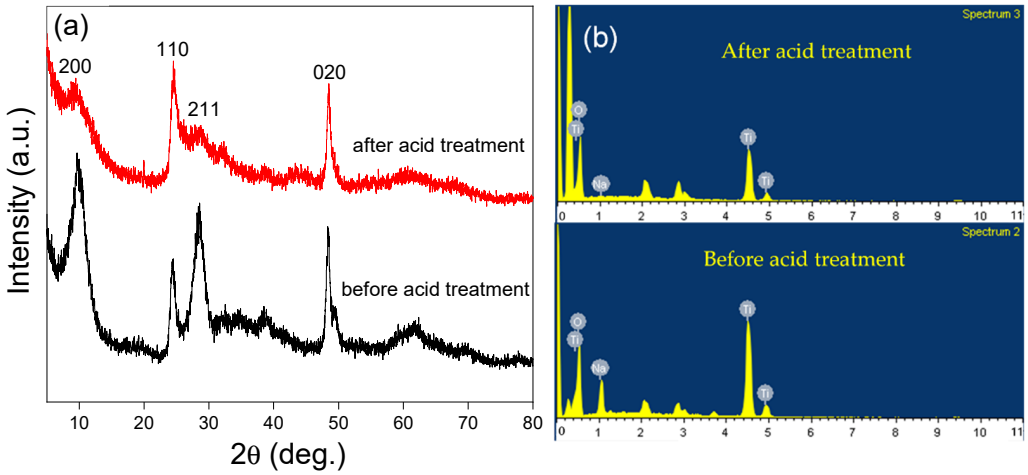

Figure 1. (**a**,**b**) Powder XRD patterns of titanate nanotubes showing the effect of acid treatment and EDX analyses before and after acid treatment.

2.1. Impact of Post-Hydrothermal Treatment on Phase Structure and Shape and Morphology

It has been demonstrated in the literature that post-hydrothermal heat treatment influences the phase, morphology and surface, consequently affecting the photocatalytic characteristics of materials [31,33]. With this view, the nanotubes were heated in an autoclave at 120 °C for different time intervals. The structural and morphological evolution as a function of heating time was investigated by XRD and FESEM. The XRD patterns of the derivatives obtained after heating the protonated tri-titanate nanotubes at 120 °C from 1 to 24 h are shown in Figure 2. As can be seen, the post-hydrothermal processing induced the structural change in nanotubes. Titanate structures undergo recrystallization and formation of TiO_2 (anatase phase) was recorded. This change was indicated by the shift in $2\theta = 24^\circ$ to a higher value. An increase in the heating time improved the crystallinity. These findings suggested that the structure of the protonated nanotubes is tri-titanate formed by the sharing of $Ti_3O_7^{2-}$ units of adjacent layers of $H_2Ti_3O_7$ [31]. These structural changes are presumably being attributed to the ion-exchange process, in which the H^+ replaced the Na^+. Under thermal activation, the presence of H^+ allows the acid-catalyzed condensation of OH groups and formation of water molecules as shown in equation below:

$$H_2Ti_3O_7 \rightarrow 3TiO_2 + H_2O$$

The dehydration process among the titanate layers may be followed by an in-situ rearrangement of the structural unites. The transformation from titanate to anatase seems to be a topotactic phase transition, which demands low energy to break the bonding in titanate leading to the formation of the anatase phase [34].

Transmission Electron Micrograph (TEM) of protonated nanotubes was also obtained and is illustrated in Figure 3. Microscopic images indicate that both the ends of the nanotubes are open, non-seamless and multiwalled. The outer diameter was calculated to be in the range of 6 to 10 nm, while the inner diameter was between 4 and 6 nm. The lengths were seen to be several hundreds of nanometers. The TEM irradiation can affect the morphology and structure of TiO_2 nanotubes, particularly the amorphous phase of TiO_2 nanotubes [35,36]. During TEM analysis, we did not observe any morphological or structural changes, presumably due to the fact that the titanate nanotubes are crystalline in nature as indicated by the XRD patterns (Figure 1). The FESEM images of both as-prepared and acid-treated products did not indicate any modification in shape and morphology because of acid treatment. The shape and morphological changes in nanotubes occurring during post-hydrothermal processing were analyzed by FESEM. The images are presented in Figure 4. The processing was carried out at 120 °C for 1, 3, 6, 12, 18 and 24 h. The images suggest that the nanotubes begin to lose their shape and morphology, and convert

into nanoparticles when heated in an autoclave at 120 °C. Similar structural evolution is observed earlier when TiO_2 nanotubes undergo thermal treatment [31,37–39]. The initial 1 h heat treatment has very little impact on the shape and morphology of nanotubes. However, when the sample was heated for 3 h, a major portion of the nanotubes were converted into nanoparticles and almost all the nanotubes were transformed into nanoparticles after 6 h. On the basis of FESEM and the XRD findings, it may be suggested that the nanotubes samples during heat treatment undergo rearrangement of the structural units, altering the phase as well as the shape and morphology of the samples drastically. In our previous study [31], a detailed investigation based on the change in crystal structure and shape and morphology of TiO_2-based nanotubes was carried out with respect to heat treatment in air. When the thermal stability of TiO_2-based nanotubes was compared in different media, such as air and water, the nanotubes showed significantly less stability in water as compared to air. This may be due to the enhanced dehydration process caused by acid-catalyzed condensation of OH groups by protons.

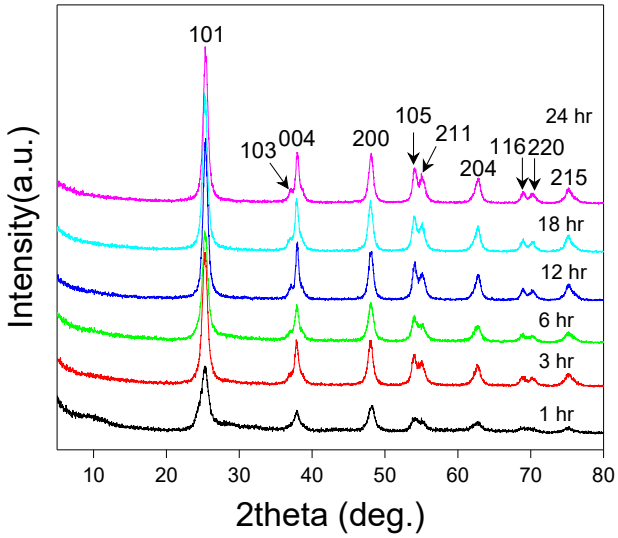

Figure 2. Powder XRD patterns of the samples obtained after post-hydrothermal heat treatment of nanotubes at 120 °C for different time periods.

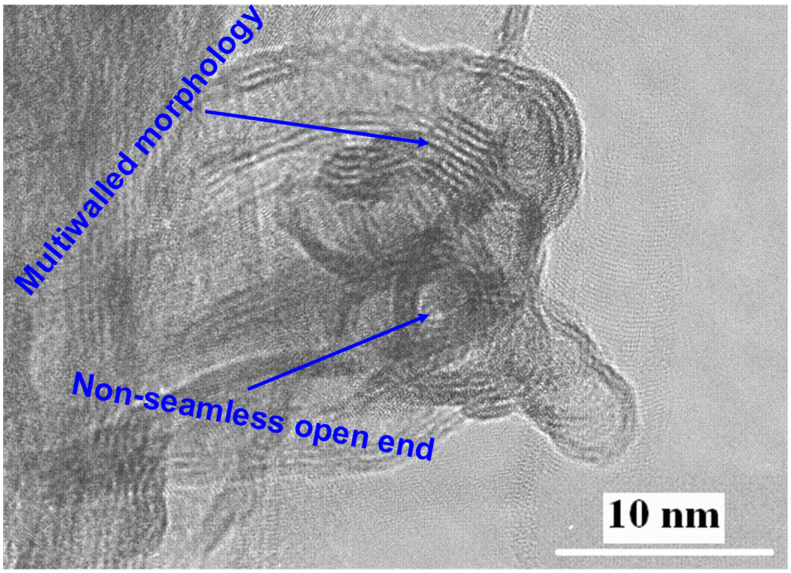

Figure 3. TEM of acid treated nanotubes showing the non-seamless open ends and multiwalled morphology.

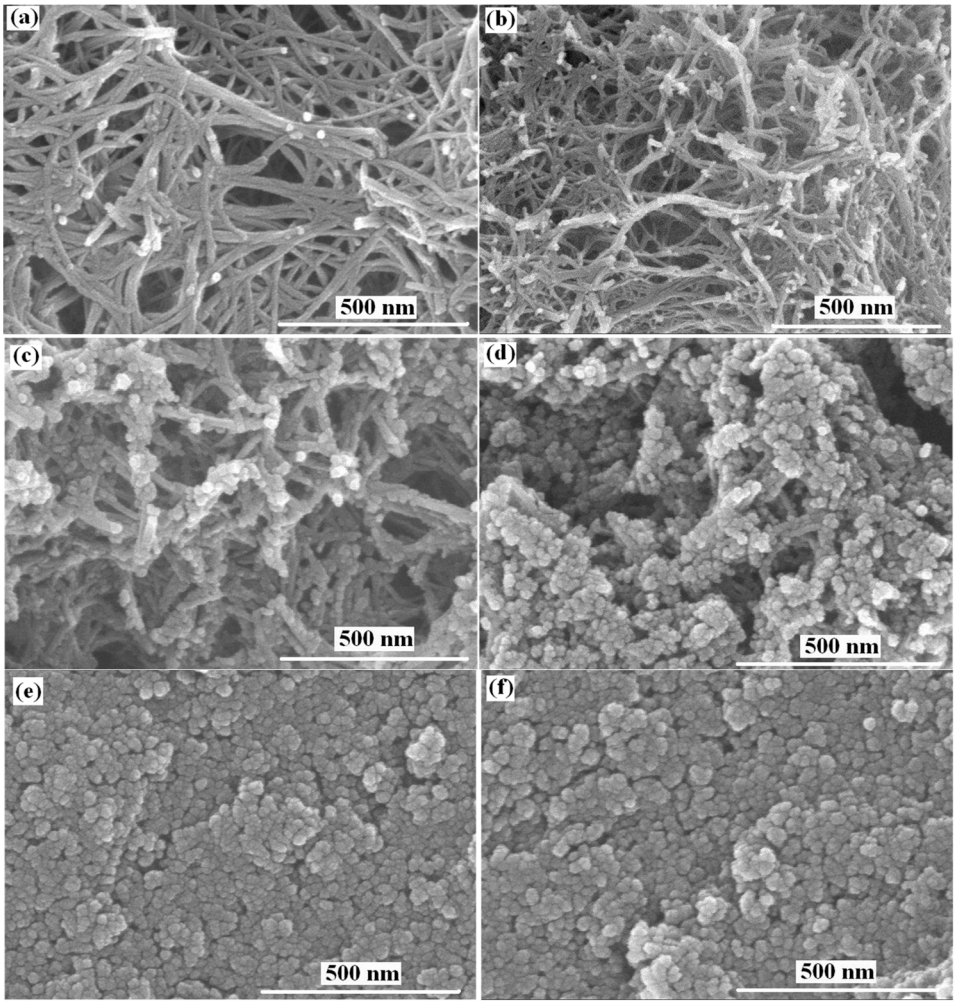

Figure 4. FESEM micrographs of nanotubes hydrothermally heated at 120 °C for different durations; (**a**) as-prepared (acid-treated) nanotubes, (**b**) 1 h, (**c**) 3 h, (**d**) 6 h, (**e**) 12 h, and (**f**) 18 h.

2.2. Impact of Post-Hydrothermal Processing on Photocatalytic Activity

In addition to structural and morphological changes, variations in the photocatalytic performance of nanotubes as a function of hydrothermal processing time were studied. This was carried out by monitoring the removal or degradation rate of amaranth. The results rates are presented in Figure 5. The values of crystallite size and surface area as a function of post-hydrothermal heat treatment are listed in Table 1. As is clear from Figure 5, the heat treatment has a substantial effect on the photocatalytic activity of the samples for amaranth degradation. It is worth noting that, in the presence of thermal derivatives, the degradation of the dye was drastically improved. The improvement in photocatalytic activity is attributed to the formation of anatase phase, as confirmed by the XRD patterns. The negligible photocatalytic activity of protonated nanotubes may be due to their titanate and mostly amorphous phase. It can be observed from Figure 5 that the photocatalytic activity of the acid treated nanotubes increases with increasing the duration of heat treatment, presumably owing to the improved crystallization of anatase phase. The samples heated at 120 °C for 12 h exhibited the highest activity for the removal of amaranth, followed by a decrease at longer heat treatment. With the increase in heating time, the surface area decreased while the anatase crystallite size increased. Despite the high surface area, the low activity shown by the sample treated for a shorter time can be rationalized to: (1) smaller fraction of photocatalytically-active anatase phase; and (2) poor crystallinity. Although the crystallinity of the samples improved with increasing heating duration, such as 18 and 24 h, the photocatalytic performance of the samples decreased. The

decrease in activity can be attributed to a decrease in surface area of the samples. It seems reasonable to infer that an optimal compromise between surface area and crystallinity should be achieved for the highest activity. This was noticed in the sample heated for 12 h. The highest photocatalytic activity shown by samples heated for 12 h can be attributed to an optimal synergistic effect of surface area and crystallinity.

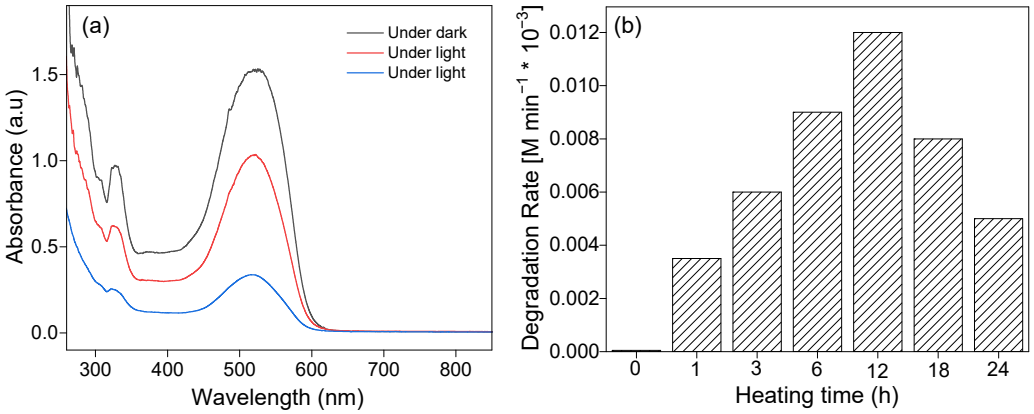

Figure 5. (**a**) Change in absorption spectra of amaranth before and after photocatalytic reaction and (**b**) change in degradation rates in the presence of nanotubes and samples obtained after post-hydrothermal heat treatment at 120 °C for different time intervals.

Table 1. BET and anatase crystallite size of as-prepared and heat-treated samples.

Sample	BET Surface Area (m^2g^{-1})	Anatase Crystallite Size (nm)
As-prepared	254	*
Acid-treated	353	*
1 h	262	~6
3 h	182	~14
6 h	119	~21
12 h	107	~25
18 h	94	~28
24 h	92	~32

*—Anatase phase was absent.

Since the highest photocatalytic activity was obtained with the sample prepared at 120 °C for 12 h, it was used for the study of photodegradation of amaranth in aqueous suspensions under a variety of experimental parameters.

2.3. Impact of pH on the Degradation Rate

The pH of the solution is a critical parameter as it affects the surface charge properties of the photocatalyst and the size of aggregates it forms. The removal of amaranth was investigated at different pH values between 3 and 10.4. The degradation rate as a function of reaction pH is summarized in Table 2. The experimental results showed that the solution pH had less impact on the degradation of dye. The degradation increased slightly with the increase in pH followed by a decrease at higher pH (e.g., 10.4). These results can be explained in terms of zero point charge (pH_{zpc}) of TiO_2 at pH ~6.5, below which the TiO_2 nanotubes are positively charged. Beyond pH 6.5, the TiO_2 nanotubes possess negative charges and the formation of OH^- by catalyst generates unfavorable repulsive forces. As a result, amaranth removal decreased at higher pH. Furthermore, the presence of a higher number of OH^- in the photocatalytic solution at higher pH might be excluded (screened) in UV analysis.

Table 2. Photocatalytic degradation of amaranth in aqueous suspensions under different experimental conditions.

Parameter	Value	Degradation Rates [M $min^{-1} \times 10^{-3}$]
Solution pH	3.5	0.0120
	5.6	0.0144
	7.9	0.0183
	10.4	0.0156
Substrate concentration (mM)	0.15	0.0120
	0.25	0.0167
	0.35	0.0268
	0.50	0.0323
	0.70	0.0231
Catalyst loading (g L^{-1})	0.5	0.0080
	1.0	0.0120
	2.0	0.0157
	3.0	0.0198
	4.0	0.0212
	5.0	0.0215

2.4. Impact of pH on the Degradation Rate

Dye or substrate concentration is another critical factor that can influence the photocatalyst's activity. It is vital to examine the relationship of the photocatalytic reaction rate on substrate concentrations. With this view, the effect of amaranth concentration ranging from 0.15 to 0.70 mM on the degradation rate was investigated. The results are summarized in Table 2. It is clear from the obtained data that the degradation rate improves with the increase in substrate concentration from 0.15 to 0.50 mM followed by decrease at higher amaranth concentration. An increase in the dye concentration increases the availability of dye molecules onto the surface of photocatalyst, leading to higher degradation. However, a highly concentrated solution of dye can produce intense color, which can prevent the light penetration into the solution or catalyst's surface. This can severely limit the surface–photon interaction, absorption, activation and production of reactive species onto the surface of the photocatalyst. As a result, the removal of amaranth decreased its concentration exceeded the optimum limit of 0.50 mM.

2.5. Impact of Photocatalyst Loading on the Degradation Rate

Optimum photocatalyst loading is another important experimental parameter that was investigated by varying photocatalyst amount between 0.5 and 5.0 g L^{-1}. The obtained values are presented in Table 2. As expected, the removal of amaranth was enhanced with the increase in photocatalyst amount, indicating typical heterogeneous catalysis behavior as reported in earlier studies [40,41]. An increase in the photocatalyst amount is expected to provide enhanced photocatalytic active centers for photon absorption and generation of reactive radicals, leading to improved removal of amaranth molecules.

The representative photocatalytic experiment (photocatalyst amount = 1 g L^{-1}, amaranth concentration = 0.15 mM, solution pH = 3.5) was repeated three times to obtain measurement error. The variation in results was found to be approximately ±2%.

2.6. Role of Conduction Band Electrons/$O_2^{-\bullet}$ and Holes/$OH^{\bullet}$

When the surface of photocatalysts is illuminated with appropriate photonic energy (equal to or greater than the band gap), an exciton (e^- and h^+ pair) could be generated. Excited conduction band electrons could readily reduce O_2 to $O_2^{-\bullet}$ while the holes in the valence band can oxidize water, generating $OH^{\bullet}$ radicals. These radical species are very reactive, though short-lived, and capable of degrading of organic molecules. To determine the role of conduction band electron/$O_2^{-\bullet}$, the photocatalytic removal of amaranth was carried out in the absence of O_2 molecules or presence of N_2 gas. Before turning on the

light, the suspension was bubbled for ~45 min with N_2 gas to ensure the removal of air and dissolved O_2. The N_2 gas bubbling was maintained throughout the reaction. The involvement of valence band holes/$OH^{\bullet}$ was also investigated by conducting the photocatalytic experiment in the presence of a hole scavenger, ammonium oxalate ($(NH_4)_2C_2O_4$). The results are shown in Figure 6a. As can be seen, the removal of amaranth was noticeably dependent on the ambient environment. The removal of the dye in the absence of oxygen was slow. This suggested that O_2 served as effective conduction band electron acceptor thereby increasing the photocatalytic removal of amaranth. Similarly, the photocatalytic removal of amaranth was decreased in the presence of the $(NH_4)_2C_2O_4$) hole scavenger. It can be noted that the effect of the hole scavenger was more profound as compared to O_2, indicating that the holes or $OH^{\bullet}$ formed during the photocatalytic reaction played a more dominant role in the removal of amaranth dye.

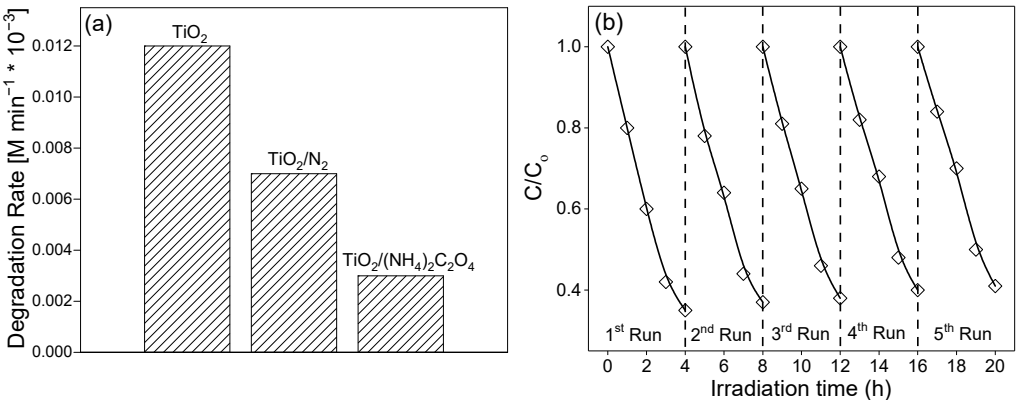

Figure 6. (**a**) Effect of O_2 and hole scavenger on the photocatalytic removal of amaranth and (**b**) effect of recycling on the photocatalytic performance.

To investigate the stability and the recyclability of the representative photocatalytic sample, photocatalytic experiments were carried out at pH = 3.5 with catalyst loading = 1 g L^{-1} and dye concentration = 0.15 mM. After the completion of each cycle, the photocatalyst was collected, washed, dried at an elevated temperature, and utilized for the next cycle under the identical photocatalytic reaction conditions. The results for five cycles (runs) are given in Figure 6b. As can be seen, the photocatalyst is stable and recyclable for the removal of amaranth.

Table 3 compares the photocatalytic results obtained in this study with those reported in the literature.

Table 3. Summary of some studies focusing on semiconductor photocatalysis for the degradation of organic pollutants.

Catalyst	Catalyst Loading	Pollutant	Pollutant Concentration	Rate/Degradation Rate	References
TiO_2 (P25)	1.0 g L^{-1}	Tebuthiuron	0.5 mM	0.012×10^{-3} M min^{-1}	[42,43]
TiO_2 (UV100)	1.0 g L^{-1}	Tebuthiuron	0.5 mM	0.004×10^{-3} M min^{-1}	[42,43]
TiO_2 (UV100)	1.0 g L^{-1}	Propachlor	0.6 mM	0.0016×10^{-3} M min^{-1}	[42,43]
TiO_2 (P25)	1.0 g L^{-1}	Chlortoluron	0.25 mM	0.013×10^{-3} M min^{-1}	[42,44]
TiO_2 (UV100)	1.0 g L^{-1}	Chlortoluron	0.25 mM	0.004×10^{-3} M min^{-1}	[42,44]
TiO_2 (PC500)	1.0 g L^{-1}	Chlortoluron	0.25 mM	0.002×10^{-3} M min^{-1}	[42,44]
TiO_2 (UV100)	1.0 g L^{-1}	Bromothymol Blue	0.25 mM	0.009×10^{-3} M min^{-1}	[42,45]
TiO_2 (P25)	1.0 g L^{-1}	5-Bromouracil	1.0 mM	0.0028×10^{-3} M min^{-1}	[42,46]
TiO_2 nanoparticles	0.1 g L^{-1}	Methylene blue	0.09 mM	7.0×10^{-4} min^{-1}	[47]
TiO_2 (P25)	0.4 g L^{-1}	Paracetamol	0.25 mM	1.9×10^{-3} min^{-1}	[48]
TiO_2 (P25)	1.0 g L^{-1}	Salicylic acid	0.1 mM	1.9×10^{-6} M min^{-1}	[49]

Table 3. *Cont.*

Catalyst	Catalyst Loading	Pollutant	Pollutant Concentration	Rate/Degradation Rate	References
TiO_2 (anatase)	0.5 g L^{-1}	Salicylic acid	0.36 mM	1.7×10^{-3} min^{-1}	[50]
Hollow mesoporous TiO_2 microspheres	0.1 g L^{-1}	Acetaminophen	0.33 mM	4.3×10^{-2} min^{-1}	[51]
TiO_2–Pd	1 g L^{-1}	Diclofenac	0.17 mM	5.0×10^{-2} min^{-1}	[52]
TiO_2–Ag				4.0×10^{-2} min^{-1}	
Graphene/TiO_2-Ag composites	4 mg	Amaranth	0.02 mM	5.8×10^{-2} min^{-1}	[53]
TiO_2 nanoparticles	1.0 g L^{-1}	Acid Blue-29	0.06 mM	0.6×10^{-4} M min^{-1}	[54]
CdS	1.0 g L^{-1}	Acid Blue-29	0.06 mM	4.5×10^{-4} M min^{-1}	[54]
CdS-TiO_2	1.0 g L^{-1}	Acid Blue-29	0.06 mM	5.8×10^{-4} M min^{-1}	[54]
Ag–TiO_2 nanofibers	0.4 g L^{-1}	Methylene blue dye	0.03 mM	1.29×10^{-2} min^{-1}	[12]
TiO_2-based nanotubes	1.0 g L^{-1}	Amaranth	0.15 mM	0.012×10^{-3} M min^{-1}	[This study]

3. Materials and Methods

3.1. Synthesis

The TiO_2 precursor was synthesized as reported in our previous work [26]. Briefly, the TiO_2 precursor was heated for 5 h in an autoclave reactor (5000 cm^3 capacity) at 150 °C under 100 bar of N_2 pressure. After that, a little portion of TiO_2 sol was mixed with 10 M NaOH and the resultant mixture was placed in a Ni-lined hydrothermal vessel. The heat treatment was carried out at 150 °C for 48 h. After reaction, white product was obtained at the bottom of the vessel. The liquid solution was discarded and the solid part was first washed with deionized water and then vigorously stirred with 0.1 N HCl at 40 °C to thoroughly eliminate the Na^+. Then, the product was extensively washed with deionized water until it was free from chloride ions. Finally, the product was filtered, treated with liquid nitrogen and freeze-dried at −57 °C. A small amount of the dried powder was suspended in water (80 mL), stirred for a long time and then transferred to the autoclave and heated at 120 °C for different time intervals.

3.2. Structural Characterization

Different characterization techniques, such as Transmission Electron Microscopy (TEM, JEM 2010, JEOL Ltd., Tokyo, Japan), Scanning Electron Microscopy (SEM, Hitachi S-4700, Tokyo, Japan), Powder X-ray Diffraction (PXRD, with Cu Kα radiation, Siemens-D50050D, Munich, Germany), and a Brunauer–Emmett–Teller surface area analyzer (BET, KICT-SPA3000, MiraeSI Co., Ltd, Gwangju, Korea), were employed to obtain sample information. The Debye–Scherrer equation was used to confirm the (anatase) crystallite size. The main diffraction pattern of anatase phase centered $2\theta = 101°$ was used.

3.3. Evaluation of Photocatalytic Activity

For the photocatalytic reactions, the catalyst (1 g L^{-1} unless stated otherwise) was added into a Pyrex photocell containing the desired concentration in 500 mL aqueous solution of the dye. The suspension was agitated magnetically for at least 30 min in the dark. This can facilitate the suspension attaining the equilibrium that is necessary in order to account for the lost compounds (due to adsorption of amaranth) during analyses. The absorption spectra recorded before and after stirring were similar, suggesting that the nanotube sample did not have noticeable adsorption capacity toward amaranth dye. The samples were irradiated using ultraviolet radiation, and dye solutions were withdrawn from the cell using a syringe before and after specific reaction times. Before turning on the light, the dye solution was withdrawn and was used as a standard dye solution to compare the concentration of irradiated dye samples.

The degradation rate for the amaranth dye was calculated following the change in absorbance at λ = ~518 nm. The rate constant of each experiment was determined from

the initial slope obtained from a plot of the absorbance (ln) vs. reaction time. Finally, the degradation rates were expressed in mol·min^{-1}.

4. Conclusions

The effect of post-hydrothermal treatment on the properties (e.g., phase, shape and morphology, textural properties, photocatalytic activity) of the nanotubes, obtained through an alkali chemical process, was investigated. It was found that the protonated titanate phase of the nanotubes transformed into anatase phase when hydrothermally heated in an autoclave at 120 °C for a certain time period. The post–hydrothermal treatment, at the same time, destructed the tubular morphology and shape, and significantly affected the crystallite size and textural properties of the nanotubes. With increasing post-hydrothermal heating time, the specific surface area was found to decrease while the crystallinity was improved. The as-prepared and acid-treated nanotubes were photocatalytically inactive, and the generation of photocatalytic activity was because of the formation of active anatase phase as a result of post-hydrothermal heat treatment. The highest photocatalytic activity was recorded because of a synergistic effect operative between surface area and crystallinity. The highest removal of amaranth was obtained at pH ~7.9 with its 0.5 mM concentration. The removal of amaranth increased with the increase in photocatalyst amount from 0.5 to 5.0 g L^{-1}. The role of holes/$OH^{\bullet}$ is more prominent as compared to that of the conduction band electrons/$O_2^{-\bullet}$ for the removal of the dye. In addition, the photocatalyst was found to be stable and recyclable.

Author Contributions: Conceptualization, M.Q. (Mohammad Qamar) and S.-J.K.; Formal analysis, M.Q. (Mohammad Qamar) and S.A.Z.; Investigation, Q.A.D. and M.Q. (Mohammad Qamar); Methodology, M.Q. (Mohammad Qamar), S.-J.K., Q.A.D. and M.Q. (Mohammad Qutob); Supervision, M.Q. (Mohammad Qamar) and S.-J.K.; Writing original draft, M.Q. (Mohammad Qutob) and S.A.Z.; Review & editing, M.Q. (Mohammad Qamar), M.R. and S.-J.K.; Funding acquisition, M.Q. (Mohammad Qamar) and M.R. All authors have read and agreed to the published version of the manuscript.

Funding: The authors would like to express their appreciation to Ministry of Higher Education Malaysia for Fundamental Research Grant Scheme with Project Code: FRGS/1/2019/STG07/USM/02/12.

Data Availability Statement: The data that support the findings of this study are available from the corresponding author upon reasonable request.

Acknowledgments: The authors acknowledge the support provided by Universiti Sains Malaysia (USM) and Interdisciplinary Research Center for Hydrogen and Energy Storage, King Fahd University of Petroleum & Minerals (KFUPM), Saudi Arabia.

Conflicts of Interest: The authors declare no conflict of interest.

References

1. Everhart, B.M.; McAuley, B.; Mayyahi, A.A.; Tonyali, B.; Yucel, Y.; Amama, P.B. Photocatalytic NO_x mitigation under relevant conditions using carbon nanotube-modified titania. *Chem. Eng. J.* **2022**, *446*, 136984. [CrossRef]
2. Li, L.; Xiao, S.; Li, R.; Cao, Y.; Chen, Y.; Li, Z.; Li, G.; Li, H. Nanotube array-like WO_3 photoanode with dual-layer oxygen-evolution cocatalysts for photoelectrocatalytic overall water splitting. *ACS Appl. Energy Mater.* **2018**, *1*, 6871–6880. [CrossRef]
3. He, Q.; Qiao, S.; Zhou, Y.; Vajtai, R.; Li, D.; Ajayan, P.M.; Ci, L.; Song, L. Carbon nanotubes-based electrocatalysts: Structural regulation, support effect, and synchrotron-based characterization. *Adv. Func. Mater.* **2022**, *32*, 2106684. [CrossRef]
4. Chang, K.C.; Zhou, Q.; Liu, K.; Li, L.; Zhang, R.; Liu, H.-J.; Kuo, T.-P. Eco-friendly, highly efficient ethanol-assisted supercritical preparation of an ultrathin ZnO nanotube. *ACS Sustain. Chem. Eng.* **2021**, *9*, 15478–15483. [CrossRef]
5. Ivanoskii, A.L. Non-carbon nanotubes: Synthesis and simulation. Russ. *Chem. Rev.* **2022**, *71*, 175–194.
6. Rempel, A.A.; Valeeva, A.A.; Vokhmintsev, A.S.; Weinstein, I.A. Titanium dioxide nanotubes: Synthesis, structure, properties and applications. *Russ. Chem. Rev.* **2021**, *90*, 1397. [CrossRef]
7. Liu, N.; Chen, X.; Zhang, J.; Schwank, J.W. A review on TiO_2-based nanotubes synthesized via hydrothermal method: Formation mechanism, structure modification, and photocatalytic applications. *Catal. Today* **2014**, *225*, 34–51. [CrossRef]
8. Humayun, M.; Raziq, F.; Khan, A.; Luo, W. Modification strategies of TiO_2 for potential applications in photocatalysis: A critical review. *Green Chem. Lett. Rev.* **2018**, *11*, 86–102. [CrossRef]
9. Humayun, M.; Wang, C.; Luo, W. Recent progress in the synthesis and applications of composite photocatalysts: A critical review. *Small* **2022**, *6*, 2101395. [CrossRef]

10. Mohamedkhair, A.K.; Drmosh, Q.A.; Qamar, M.; Yamani, Z.H. Tuning structural properties of WO_3 thin films for photoelectrocatalytic water oxidation. *Catalysts* **2021**, *11*, 381. [CrossRef]
11. Drmosh, Q.A.; Hezam, A.; Hossain, M.K.; Qamar, M.; Yamani, Z.H.; Byrappa, K. A novel Cs_2O–Bi_2O_3–TiO_2–ZnO heterostructure with direct Z-Scheme for efficient photocatalytic water splitting. *Ceram. Int.* **2019**, *45*, 23756–23764. [CrossRef]
12. Pascariu, P.; Cojocaru, C.; Airinei, A.; Olaru, N.; Rosca, I.; Koudoumas, E.; Suchea, M.P. Innovative Ag–TiO_2 nanofibers with excellent photocatalytic and antibacterial actions. *Catalysts* **2021**, *11*, 1234. [CrossRef]
13. Tsebriienko, T.; Popov, A.I. Effect of poly(titanium oxide) on the viscoelastic and thermophysical properties of interpenetrating polymer networks. *Crystals* **2021**, *11*, 794. [CrossRef]
14. Badmus, K.O.; Wewers, F.; Al-Abri, M.; Shahbaaz, M.; Petrik, L.F. Synthesis of oxygen deficient TiO_2 for improved photocatalytic efficiency in solar radiation. *Catalysts* **2021**, *11*, 904. [CrossRef]
15. Gyulavári, T.; Dusnoki, D.; Márta, V.; Yadav, M.; Abedi, M.; Sápi, A.; Kukovec, A.; Kónya, Z.; Pap, Z. Dependence of photocatalytic activity on the morphology of strontium titanates. *Catalysts* **2022**, *12*, 523. [CrossRef]
16. Li, D.; Song, H.; Meng, X.; Shen, T.; Sun, J.; Han, W.; Wang, X. Effects of particle size on the structure and photocatalytic performance by alkali-treated TiO_2. *Nanomaterials* **2020**, *10*, 546. [CrossRef]
17. Armstrong, G.; Armstrong, A.R.; Canales, J.; Bruce, P.G. Nanotubes with the TiO_2-B structure. *Chem. Commun.* **2005**, *19*, 2454–2456. [CrossRef]
18. Armstrong, A.R.; Armstrong, G.; Canales, J.; Garcia, R.; Bruce, P.G. Lithium-ion intercalation into TiO_2-B nanowires. *Adv. Mater.* **2005**, *17*, 862–865. [CrossRef]
19. Wu, Z.; Hwang, I.; Cha, G.; Qin, S.; Tomanec, O.; Badura, Z.; Kment, S.; Zboril, R.; Schmuki, P. Optimized Pt single atom harvesting on TiO_2 nanotubes—Towards a most efficient photocatalyst. *Small* **2022**, *18*, 2104892. [CrossRef]
20. Lv, Y.; Wu, X.; Lin, H.; Li, J.; Zhang, H.; Guo, J.; Jia, D.; Zhang, H. A novel carbon support: Few-layered graphdiyne-decorated carbon nanotubes capture metal clusters as effective metal-supported catalysts. *Small* **2021**, *17*, 2006442. [CrossRef]
21. Wiel, L.; Li, H.; Rust, C.; Chen, J.; Flavel, B.S. Carbon nanotubes for photovoltaics: From lab to industry. *Adv. Energy Mater.* **2021**, *11*, 2002880.
22. Kasuga, T.; Hiramatsu, M.; Hoson, A.; Sekino, T.; Niihara, K. Formation of titanium oxide nanotube. *Langmuir* **1998**, *14*, 3160–3163. [CrossRef]
23. Gautam, J.; Yang, J.-M.; Yang, B.l. Transition metal co-doped TiO_2 nanotubes decorated with Pt nanoparticles on optical fibers as an efficient photocatalyst for the decomposition of hazardous gaseous pollutants. *Colloid Surf. A* **2022**, *643*, 128786. [CrossRef]
24. Kim, E.; Do, K.H.; Wang, J.; Hong, Y.; Rangappa, A.P.; Reddy, D.A.; Kumar, D.P.; Kim, T.K. Construction of 1D TiO_2 nanotubes integrated ultrathin 2D $ZnIn_2S_4$ nanosheets heterostructure for highly efficient and selective photocatalytic CO_2 reduction. *App. Surf. Sci.* **2022**, *587*, 152895. [CrossRef]
25. Wang, H.; Li, H.; Chen, Z.; Li, J.; Li, X.; Huo, P.; Wang, Q. TiO_2 modified g-C_3N_4 with enhanced photocatalytic CO_2 reduction performance. *Solid State Sci.* **2020**, *100*, 106099. [CrossRef]
26. Fabrication of PbS nanocrystal-sensitized ultrafine TiO_2 nanotubes for efficient and unusual broadband-light-driven hydrogen production. *Mater. Today Chem.* **2020**, *17*, 100310. [CrossRef]
27. Guo, J.Q.; Fan, Y.-P.; Dong, X.-S.; Ma, X.-M.; Yao, S.-L.; Xing, H.-J. Modified coal tailings with TiO_2 nanotubes and their application for methylene blue removal. *Colloid Surf. A* **2021**, *627*, 127211. [CrossRef]
28. Liu, W.; Borthwick, A.G.L.; Li, X.Z.; Ni, J.R. High photocatalytic and adsorptive performance of anatase-covered titanate nanotubes prepared by wet chemical reaction. *Micropor. Mesopor. Mater.* **2014**, *186*, 168–175. [CrossRef]
29. Cheng, K.; Cai, Z.; Fu, J.; Sun, X.; Sun, W.; Chen, L.; Zhang, D.; Liu, W. Synergistic adsorption of Cu (II) and photocatalytic degradation of phenanthrene by a jaboticaba-like TiO_2/titanate nanotube composite: An experimental and theoretical study. *Chem. Eng. J.* **2019**, *358*, 1155–1165. [CrossRef]
30. Zhao, X.; Cai, Z.; Wang, T.; O'Reilly, S.; Liu, W.; Zhao, D. A new type of cobalt-deposited titanate nanotubes for enhanced photocatalytic degradation of phenanthrene. *Appl. Catal. B Environ.* **2016**, *187*, 134–143. [CrossRef]
31. Qamar, M.; Yoon, C.R.; Oh, H.J.; Kim, D.H.; Jho, J.H.; Lee, K.S.; Lee, W.J.; Lee, H.G.; Kim, S.J. Effect of post treatments on the structure and thermal stability of titanate nanotubes. *Nanotechnology* **2006**, *17*, 5922–5929. [CrossRef]
32. Bavykin, D.V.; Friedrich, J.M.; Walsh, F.C. Protonated titanates and TiO_2 nanostructured materials: Synthesis, properties, and applications. *Adv. Mater.* **2006**, *18*, 2807–2824. [CrossRef]
33. Qamar, M.; Yoon, C.R.; Oh, H.J.; Lee, N.H.; Park, K.; Kim, D.H.; Lee, K.S.; Lee, W.J.; Kim, S.J. Preparation and photocatalytic activity of nanotubes obtained from titanium dioxide. *Catal. Today* **2008**, *131*, 3–14. [CrossRef]
34. Zhu, H.Y.; Gao, X.P.; Lan, Y.; Song, D.Y.; Xi, Y.X.; Zhao, J.C. Hydrogen titanate nanofibers covered with anatase nanocrystals: A delicate structure achieved by the wet chemistry reaction of the titanate nanofibers. *J. Am. Chem. Soc.* **2004**, *126*, 8380–8381. [CrossRef]
35. Yang, C.; Olsen, T.; Lau, M.L.; Smith, K.A.; Hattar, K.; Sen, A.; Xiong, H. In situ ion irradiation of amorphous TiO_2 nanotubes. *J. Mater. Res.* **2022**, *37*, 1144–1155. [CrossRef]
36. Zhukovskii, Y.F.; Pugno, N.; Popov, A.I.; Balasubramanian, C.; Bellucci, S. Influence of F centres on structural and electronic properties of AlN single-walled nanotubes. *J. Phys. Condens. Matter* **2007**, *19*, 395021. [CrossRef]
37. Zavala, M.Á.L.; Morales, S.A.L.; Ávila-Santos, M. Synthesis of stable TiO_2 nanotubes: Effect of hydrothermal treatment, acid washing and annealing temperature. *Heliyon* **2017**, *3*, e00456. [CrossRef]

38. Suzuki, Y.; Sakulkhaemaruethai, S.; Yoshida, R.; Yoshikawa, S. Heat treatment effect on the structure of TiO_2-derived nanotubes prepared by hydrothermal method. In *Ceramic Nanomaterials and Nanotechnology III, Proceedings of the 106th Annual Meeting of The American Ceramic Society, Indianapolis, Indiana, USA 2004*; John Wiley & Sons: Hoboken, NJ, USA, 2006; Volume 159, pp. 185–192.
39. J Suzuki, Y.; Yoshikawa, S. Synthesis and thermal analyses of TiO_2-derived nanotubes prepared by the hydrothermal method. *J. Mater. Res.* **2004**, *19*, 982–985. [CrossRef]
40. Qamar, M.; Muneer, M. A comparative photocatalytic activity of titanium dioxide and zinc oxide by investigating the degradation of vanillin. *Desalination* **2009**, *249*, 535–540. [CrossRef]
41. Qamar, M.; Gondal, M.A.; Yamani, Z.H. Synthesis of highly active nanocrystalline WO_3 and its application in laser-induced photocatalytic removal of a dye from water. *Catal. Commun.* **2009**, *10*, 1980–1984. [CrossRef]
42. Bahnemann, D.; Muneer, M.; Haque, M. Titanium dioxide-mediated photocatalysed degradation of few selected organic pollutants in aqueous suspensions. *Catal. Today* **2007**, *124*, 133–148. [CrossRef]
43. Muneer, M.; Qamar, M.; Saquib, M.; Bahnemann, D.W. Heterogeneous photocatalysed reaction of three selected pesticide derivatives, propham, propachlor and tebuthiuron in aqueous suspensions of titanium dioxide. *Chemosphere* **2005**, *61*, 457–468. [CrossRef] [PubMed]
44. Haque, M.M.; Muneer, M.; Bahnemann, D.W. Semiconductor-mediated photocatalyzed degradation of a herbicide derivative, chlorotoluron, in aqueous suspensions. *Environ. Sci. Technol.* **2006**, *40*, 4765. [CrossRef] [PubMed]
45. Haque, M.M.; Muneer, M. TiO_2-mediated photocatalytic degradation of a textile dye derivative, bromothymol blue, in aqueous suspensions. *Dye. Pigment.* **2007**, *75*, 443–448. [CrossRef]
46. Singh, H.K.; Saquib, M.; Haque, M.M.; Muneer, M.; Bahnemann, D.W. Heterogeneous photocatalyzed degradation of uracil and 5-bromouracil in aqueous suspensions of titanium dioxide. *J. Hazard. Mater.* **2007**, *142*, 425–430. [CrossRef]
47. Reda, S.M.; Khairy, M.; Mousa, M.A. Photocatalytic activity of nitrogen and copper doped TiO_2 nanoparticles prepared by microwave-assisted sol-gel process. *Arab. J. Chem.* **2020**, *13*, 86–95. [CrossRef]
48. Yang, L.; Yu, L.E.; Ray, M.B. Photocatalytic oxidation of paracetamol: Dominant reactants, intermediates, and reaction mechanisms. *Environ. Sci. Technol.* **2009**, *43*, 460–465. [CrossRef]
49. Mohammadi, T.; Isfahani, A.Z. Photooxidation of salicylic acid with TiO_2 and metal coated TiO_2. *Acta Chim. Slov.* **2008**, *55*, 172–178.
50. Carlotti, M.E.; Sapino, S.; Vione, D.; Minero, C.; Peira, E.; Trotta, M. Study on the photodegradation of salicylic acid in different vehicles in the absence and in the presence of TiO_2. *J. Dispers. Sci. Technol.* **2007**, *28*, 805–818. [CrossRef]
51. Lin, C.J.; Yang, W.T.; Chou, C.Y.; Liou, S.Y.H. Hollow mesoporous TiO_2 microspheres for enhanced photocatalytic degradation of acetaminophen in water. *Chemosphere* **2016**, *152*, 490–495. [CrossRef]
52. Espino-Estévez, M.R.; Fernández-Rodríguez, C.; González-Díaz, O.M.; Araña, J.; Espinós, J.P.; Ortega-Méndez, J.A.; Doña-Rodríguez, J.M. Effect of TiO_2-Pd and TiO_2-Ag on the photocatalytic oxidation of diclofenac, isoproturon and phenol. *Chem. Eng. J.* **2016**, *298*, 82–95. [CrossRef]
53. Roşu, M.C.; Socaci, C.; Floare-Avram, V.; Borodi, G.; PogĂcean, F.; Coroş, M.; MĂgeruşan, L.; Pruneanu, S. Photocatalytic performance of graphene/TiO_2-Ag composites on amaranth dye degradation. *Mater. Chem. Phys.* **2016**, *179*, 232–241. [CrossRef]
54. Qutub, N.; Singh, P.; Sabir, S.; Sagadevan, S.; Oh, W.-C. Enhanced photocatalytic degradation of Acid Blue dye using CdS/TiO_2 nanocomposite. *Sci. Rep.* **2022**, *16*, 5759. [CrossRef] [PubMed]